Redox Biology 58 (2022) 102519

Contents lists available at ScienceDirect

Redox Biology

journal homepage: www.elsevier.com/locate/redox

# Cystathionine γ lyase S-sulfhydrates Drp1 to ameliorate heart dysfunction

Dan Wu [c], Bo Tan [d], Yuanyuan Sun [a,b], Qingxun Hu [a,b,*]

[a] Institute of Geriatrics (Shanghai University), Affiliated Nantong Hospital of Shanghai University (The Sixth People's Hospital of Nantong), School of Medicine, Shanghai University, Nantong, 226011, China
[b] Shanghai Engineering Research Center of Organ Repair, School of Medicine, Shanghai University, Shanghai, 200444, China
[c] Department of Pharmacy, Tongji Hospital, Tongji University School of Medicine, Shanghai, 200065, China
[d] Laboratory of Clinical Pharmacokinetics, Institute of Clinical Pharmacology, Shuguang Hospital Affiliated to Shanghai University of Traditional Chinese Medicine, Shanghai, 200021, China

ARTICLE INFO

*Keywords:*
Hydrogen sulfide
Dynamin related protein 1
S-Sulfhydration
Mitochondrial fission
Heart failure

ABSTRACT

Hydrogen sulfide ($H_2S$), produced by cystathionine γ lyase (CSE), is an important endogenous gasotransmitter to maintain heart function. However, the molecular mechanism for how $H_2S$ influences the mitochondrial morphology during heart failure remains poorly understood. Here, we found that CSE/$H_2S$ pathway mediated cardiac function and mitochondrial morphology through regulating dynamin related protein 1 (Drp1) activity and translocation. Mechanistically, elevation of $H_2S$ levels by CSE overexpression declined protein level, phosphorylation (Ser 616), oligomerization and GTPase activity of Drp1 by S-sulfhydration in mouse hearts. Interestingly, Drp1 S-sulfhydration directly competed with S-nitrosylation by nitric oxide at the specific cysteine 607. The non-S-sulfhydration of Drp1 mutation (C607A) attenuated the regulatory effect of $H_2S$ on Drp1 activation, mitochondrial fission and heart function. Moreover, the non-canonical role of Drp1 mediated isoprenaline-induced mitochondrial dysfunction and cardiomyocyte death through interaction with voltage-dependent anion channel 1. These results uncover that a novel mechanism that $H_2S$ S-sulfhydrated Drp1 at cysteine 607 to prevent heart failure through modulating its activity and mitochondrial translocation. Our findings also provide initial evidence demonstrating that Drp1 may be a critical regulator as well as an effective strategy for heart dysfunction.

## 1. Introduction

Cardiovascular disease remains a leading cause of death in the world [1]. As the increase in aging population, cardiovascular risk factors and improved treatment therapies for ischemic heart events, the prevalence of heart failure is steadily rising to approximately 64.3 million people worldwide with extra millions of undiagnosed cases, describing it as global pandemic [2]. Although significant advances in pharmacological treatments and the use of guideline-directed therapies for patients with heart failure, the morbidity and mortality of heart failure associated with the condition remain unacceptably high. However, there have been few new medical strategies for heart failure in the past twenty years [3,4]. The novel concept and therapy for heart failure treatment are urgently needed.

The heart is a high energy demand organ and consumes the majority of adenosine triphosphate (ATP) (~95%) that is derived from oxidative metabolism in mitochondria. Mitochondrial dysfunction contributes to the development of heart failure through multiple mechanisms, such as bottlenecks of metabolic flux, impaired $Ca^{2+}$ homeostasis, redox imbalance, protein modification and so on [5,6]. In addition, mitochondrial dynamics play a critical role in mitochondrial quality control and mitochondrial damage is often linked to morphological changes [7]. For instance, dynamin-related protein 1 (Drp1) deficiency caused cardiomyopathy and lethality [8–10]. We and other group previously reported that excessive lipid uptake increased Drp1 activity, led to mitochondrial fission and dysfunction in the heart [11,12]. Moreover, the non-canonical functions of Drp1, e.g. stimulating mPTP (mitochondrial permeability transition pore) opening, caused heart dysfunction in ischemia-reperfusion injury [13,14]. Therefore, a deeper understanding of the molecular mechanism by which Drp1 activation and the role of Drp1 are imperative to the development of targeted novel therapeutics for heart failure.

Hydrogen sulfide ($H_2S$) is a product of cysteine metabolism by cystathionine γ lyase (CSE) in the heart, which is a known biological active gasotransmitter [15]. Preclinical and clinical experiments show that

* Corresponding author. School of Medicine Shanghai University, 716 Jinqiu Road, Research Building, Room 215, Shanghai, 200444, China.
*E-mail address:* qingxh@shu.edu.cn (Q. Hu).

https://doi.org/10.1016/j.redox.2022.102519
Received 19 September 2022; Received in revised form 7 October 2022; Accepted 21 October 2022
Available online 28 October 2022

**Non-standard abbreviations and acronyms**

| | |
|---|---|
| ATP | Adenosine triphosphate |
| BNP | Brain natriuretic peptide |
| CSE | Cystathionine γ lyase |
| Drp1 | Dynamin related protein 1 |
| DTT | Dithiothreitol |
| EDTA | Ethylenediaminetetraacetic acid |
| EM | Electron microscopy |
| GED | GTPase effector domain |
| GTPase | Guanosine triphosphatase |
| $H_2O_2$ | Hydrogen peroxide |
| $H_2S$ | Hydrogen sulfide |
| iNOS | Inducible nitric oxide synthase |
| ISO | Isoprenaline |
| KHB | Krebs-Henseleit Buffer |
| MBB | Monobromobimane |
| mPTP | Mitochondrial permeability transition pore |
| $NAD^+$ | Nicotinamide adenine dinucleotide (oxidized) |
| NADH | Nicotinamide adenine dinucleotide (reduced) |
| NO | Nitric oxide |
| TMRM | Tetramethylrhodamine, methyl ester |
| VDAC1 | Voltage-dependent anion channel 1 |
| WT | Wild type |

endogenous $H_2S$ generation is blunted in the heart injury and the insufficient production of $H_2S$ contributes to the progression of heart diseases [16]. Restored $H_2S$ level by CSE overexpressing or exogenous sulfide-based therapies protected against in myocardial infarction and heart failure [17–19]. $H_2S$ has emerged as a key regulator via anti-apoptotic and antioxidant pathways and anti-inflammatory effects [16,20]. Increasing study reports that $H_2S$ exerts biological actions through S-sulfhydration of target proteins, whereby a sulfhydryl (-SH) group is post-translationally added to a cysteine residue [21]. This sulfhydration facilitates rapid responses and the fine tuning of cellular signaling. It has been estimated that up to 25% of proteins are S-sulfhydrated [22]. Despite the clear link to mitochondrial function, to date it has not been unraveled whether $H_2S$ directly regulates mitochondria morphology during the development of heart failure.

The aims of this study were to investigate whether $H_2S$ regulates Drp1 activity through S-sulfhydration and to decipher the mechanism by which activated Drp1 compromises cardiac hypertrophy and dysfunction. We found that CSE deficiency substantially exacerbated heart failure, whereas overexpression of CSE significantly corrected cardiac dysfunction and hypertrophy. Mechanistically, $H_2S$ competed with NO to bind the thiol group of cysteine 607 of Drp1. S-sulfhydrated Drp1 prevented its activity and translocation to mitochondria to induce mitochondrial hyperfission and heart dysfunction. In addition, Drp1 S-sulfhydraiton alleviated cardiomyocyte apoptosis through declining the interaction between Drp1 and the voltage-dependent anion channel 1 (VDAC1). The non-S-suflhydration of Drp1 (cysteine 607 mutated to alanine) blocked the protective role of $H_2S$ in heart function. These findings uncover a novel post-translational Drp1 modification by S-suflhydration, which will be a potential therapeutic target.

## 2. Methods

### 2.1. Animals

The rodents (mice and rats) were handled according to the Guide for the Care and Use of Laboratory Animals published by the National Research Council (United States) Committee. Experimental procedures were performed with the approved protocol by the Institutional Animal Care and Use Committee of Shanghai University. Both male and female mice were included in the study. The CSE KO mice (C57BL/6 background) were purchased from Shanghai Research Center for Model Organisms. Wild type mice (C57BL/6) and rats (Sprague Dawley) were purchased from Shanghai Jiesijie Laboratory Animal Company. Purified CSE or Drp1 C607A adenovirus ($1 \times 10^9$ opu) was administered by direct injection to the LV free wall (three sites, 25 μl per site) of WT mice and these mice were respectively named CSE OE mice and Drp1 C607A mice. ISO subcutaneous injection or TAC surgery was performed 5 days after adenovirus injection. All mice were kept on regular chow and water ad libitum in a vivarium with a 12 h light/dark cycle at 22 °C. Mice were euthanized with an intraperitoneal injection of a pentobarbital overdose (100 mg/kg).

### 2.2. TAC or ISO-induced heart failure

For TAC-induced heart failure, eight-week-old male mice were randomly assigned to respective groups and underwent TAC or sham surgery. Mice were anesthetized by sodium pentobarbital (75 mg/kg) and 1.5% isoflurane. Aorta was exposed through left thoracotomy and a constriction was made by using a 7-0 ligature around the vessel and tied against a 27-gauge blunt needle. The sham surgery was performed without the constriction of the aorta. For ISO-induced heart failure, mice were subcutaneously injected with 7.5 mg/kg ISO everyday to induce heart failure. The control group mice were injected subcutaneously with vehicle. After 4 weeks, hearts were harvested for further studies such as heart weight, pathological staining analysis, mitochondrial morphology by electron microscopy and protein levels by Western blots. Blinding procedures were applied in endpoint analysis on mice including mitochondrial morphology, echocardiography, pathological analysis and $H_2S$ level measurements.

### 2.3. Transthoracic echocardiography

The mice were anesthetized and maintained with 1–2% isoflurane and 95% oxygen. Echocardiograph was conducted using Vevo770 (VisualSonics) and a 30 MHz transducer. A parasternal short axis view was used to receive M-mode images for the analysis of ejection fraction, fraction shortening, left ventricular internal diameter-diastole and left ventricular end-diastolic volume.

### 2.4. Transmission electron microscopy

Hearts were excised immediately and washed in ice-cold saline. Tissues from left ventricle were collected, sectioned (80–100 nm thick) and fixed in 2.5% glutaraldehyde at 4 °C for 1 day. Mitochondrial morphologic images were done at Shanghai Institute of Precision Medicine and mitochondrion size were analyzed by blind counting. Three sections from each heart were calculated.

### 2.5. Organ weight and histological analysis

Heart weight and tibia length were detected at 12 weeks. Hearts were excised quickly, rinsed in PBS buffer, blotted dry and weighted. The heart hypertrophy was determined by heart weight to tibia length ratio. Heart tissues were rinsed with PBS and fixed in 10% formalin overnight. Fixed hearts were dehydrated, embedded in paraffin wax and sectioned for masson trichrome and hematoxylin-eosin staining. Each staining images was photographed by the Zeiss microscope and collagen content was quantified with ImageJ software by blinding.

### 2.6. $H_2S$ level measurements

The $H_2S$ level in the heart tissue were measured using the modified monobromobimane (MBB) method as described previously [23]. In brief, the heart tissues were lysed in the lysis buffer (Pierce, Cat. No. 89900). 30 μl sample was mixed with 10 μl Tris-HCl (100 mmol/L, pH = 8.5), 70 μl MBB solution (20 mmol/L) and 10 μl EDTA solution (2.0 mg/mL) at room temperature for 1 h. The derivatization reaction was stopped by adding 10 μl 20% formic acid. Then, a 10 μl $^{36}$S-labeled sulfidedibimane solution was added. After the mixture was subjected to centrifugate at 12,000 rpm for 10 min, 1 μl of the supernatant was injected into the LC–MS/MS system for analysis.

### 2.7. Adult rat cardiomyocyte isolation and treatments

Adult cardiomyocytes were isolated from Sprague Dawley rats (200–250 g, male, Shanghai Jiesijie) according to the standard enzymatic technique as described previously [24]. In brief, the heart was excised quickly from anesthetized rat, cannulated through the ascending aorta, mounted on a Langendorff equipment, and perfused with oxygenated Krebs-Henseleit Buffer (KHB) with collagenase II (Worthington, Cat No. LS004177) and hyaluronidase (Sigma, Cat No. H3506) at 37 °C. After 20 min, the perfused heart was cut into small pieces and gently swirl in 37 °C water bath. Rod shaped cardiomyocytes were collected and plated on the coverslip with pre-coated laminin (Thermo Fisher, Cat No. 23017-015). Cardiomyocytes cultured in M199 medium (Sigma, Cat. No. M2520) with 5.5 mmol/L glucose as fuel, and supplemented with 10 mmol/L glutathione, 26.2 mmol/L sodium bicarbonate, 0.02% bovine serum albumin and 50 U/ml penicillin–streptomycin for 72 h to allow adequate gene expression. Attached cardiomyocytes were infected with Ad-Drp1, Ad-Drp1 C607A, Ad-GFP-Drp1, Ad-GFP-Drp1 C607A, Ad-mt-SoNar and Ad-mt-cpYFP at a multiplicity of infection of 50–100. ISO (Sigma, Cat. No. I0599990, 10 μmol/L) incubated for 48 h. VBIT-4 (Selleck, Cat. No. S3544, 10 μmol/L) incubated for 48 h.

### 2.8. Plasmids and recombinant adenoviral vectors

The cDNA of GFP-Drp1 contains Drp1 variant from human (NCBI number NP_005681.2) fused with a N-terminal GFP tag. The cysteine 607 position is according to the human Drp1 variant. The primer sequences for the site-directed mutagenesis of Drp1 are as follows:

C300A, forward: GCTTTACCAGAGTTGAAAACAAGAA.
C300A, reverse: ATCTCTGATGTGATGCATCAGTAA.
C345A, forward: GCTAACACTATTGAAGGAACTGCAA.
C345A, reverse: ATATTCTGTGGCAAATTTGGTAATA.
C361A, forward: GCCGGTGGTGCTAGAATTTG.
C361A, reverse: TAGCTCCGAAGTTTCAATATATTTT.
C367A, forward: GCTTATATTTTCCATGAGACTTTTGG.
C367A, reverse: AATTCTAGCACCACCGCATAGC.
C431A, forward: GCTGTGGAACTGGTTCATGAGGAAAT.
C431A, reverse: GCGGAGGCTGGGCTCTTCCA.
C446A, forward: GCTAGCAATTACAGTACACAGGAATT.
C446A, reverse: GTGCTGAATGATCCTTTGCATT.
C470A, forward: GCTCTTCTTCGTAAAAGGTTGC.
C470A, reverse: AGTCACCACTTCAACTATGGCA.
C505A, forward: GCTGGGCTAATGAACAATAATATAGA.
C505A, reverse: AGCATCAGCAAAGTCTGGATGT.
C607A, forward: CTATCTGCTCGGGAACAGCGAGATGCTGAGGTTATTG.
C607A, reverse: GATTTAATGAGTCGTTCAATAACCTCAGCATCTCGCTGTTC.

The protocol of recombinant adenoviral vectors is previously described [12]. In brief, pBHGloxΔE1, 3Cre (Microbix) including ΔE1 adenoviral genome was co-transfected with pDCshuttle vector containing the target gene into HEK 293T cells by Lipofectamine 2000 (Invitrogen, Cat. No. 11668019). After homologous recombination, the target genes were integrated into the E1-deleted adenoviral genome. The viruses were propagated in HEK293T cells and purified using $CsCl_2$ banding followed by dialysis against 20 mmol/L Tris buffered saline with 2% glycerol. The virus concentrations were estimated to be ~1 × 10 [11] viral particles per ml, aliquoted and stored at −80 °C.

### 2.9. Biotin-switch analysis

The assay was performed to measure S-sulfhydration and S-nitrosylation status of Drp1 as described previously [25]. Briefly, tissues or cardiomyocytes were homogenized in HEN buffer including 250 mmol/L HEPES-NaOH (pH = 7.7), 0.1 mmol/L neocuproine and 1 mmol/L EDTA. For S-sulfhydration assay, but not S-nitrosylation assay, 100 μmol/L deferoxamine was added to HEN buffer and centrifuged at 13,000 r/min for 30 min at 4 °C. The lysates were added to blocking buffer including HEN buffer with 2.5% SDS and 20 mmol/L MMTS at 50 °C for 20 min with frequent vortex. The MMTS was then removed by acetone and proteins were precipitated at −20 °C for 20 min. After acetone removal, samples were resuspended in HENS buffer including HEN buffer with 1% SDS. Biotin-HPDP (APExBio, Catalog No. A8008, 4 mmol/L) was added into the suspension without ascorbic acid. For S-nitrosylation assay, 1 mmol/L ascorbic acid was also added to HEN buffer in this step. After incubation for 3 h at room temperature, biotinylated proteins were precipitated by streptavidin-agarose beads and washed with HENS buffer. The beads were washed 5 times with PBS buffer and spun down at 8000 rpm for 30 s. The biotinylated proteins were eluted by the loading buffer. Finally, the S-sulfhydrated Drp1 was analyzed by Westernblot with anti-Drp1 antibody.

### 2.10. Immunoblot analysis

Homogenized heart tissue and adult cardiomyocytes were lysed in the cell lysis buffer with a cocktail of proteinase/phosphate inhibitors (Cell Signaling Technology, Cat. No. 5872). Cytosolic and mitochondrial fractions were separated from heart tissue according to a previous protocol described [26]. Equal amount of proteins were subjected to SDS-PAGE followed by transferring to nitrocellulose membranes. The membranes were blocked with 5% non-fat milk including 0.1% tween-20 for 1 h at room temperature and then incubated with primary antibodies at 4 °C overnight. After washing with tris buffered saline with 0.1% tween-20 for three times, the membranes were incubated with an HRP-conjugated indicated secondary antibody. Immunoblot signal was measured by chemiluminescence method and protein abundance was analyzed densitometrically and normalized by the level of GAPDH or VDAC1. We used the following primary antibodies for Western blotting: anti-CSE (1:1000, Santa Cruz Biotechnology, Cat. No. sc-374249), anti-Drp1 (1:2000, BD Biosciences, Cat. No. 611113), anti-Phospho-Drp1 (S616) and anti-Phospho-Drp1 (S637) (1:1000, Cell Signaling Technology, Cat. No. 3455S and 6319S), anti-VDAC1 (1:1000, Proteintech, Cat. No. 55259-1-AP), anti-Bcl-2 (1:1000, Cell Signaling Technology, Cat. No. 3498S), anti-Bax (1:1000, Cell Signaling Technology, Cat. No. 2772S) anti-cleaved caspase-9 (1:1000, Cell Signaling Technology, Cat. No. 9508S), anti-iNOS (1:1000, Beyotime, Cat. No. AF7281), anti-GAPDH (1:5000, Cell Signaling Technology, Cat. No. 2118S). The appropriate secondary antibodies: goat anti-Rabbit IgG (H + L) Secondary Antibody (1:10000, Invitrogen, Cat. No. 31460) and Goat anti-Mouse IgG (H + L) Secondary Antibody (1:10000, Invitrogen, Cat. No. 31430).

### 2.11. Immunoprecipitation

The heart tissue and adult cardiomyocytes were collected in PBS with 0.1% Triton X-100 and then homogenized by ultrasonics. The lysates were centrifuged at 12,000 g for 10 min. The protein levels in the supernatants were detected by protein assay kit and then incubated with IgG or Drp1 antibody at 4 °C for overnight. The Protein A/G Magnetic

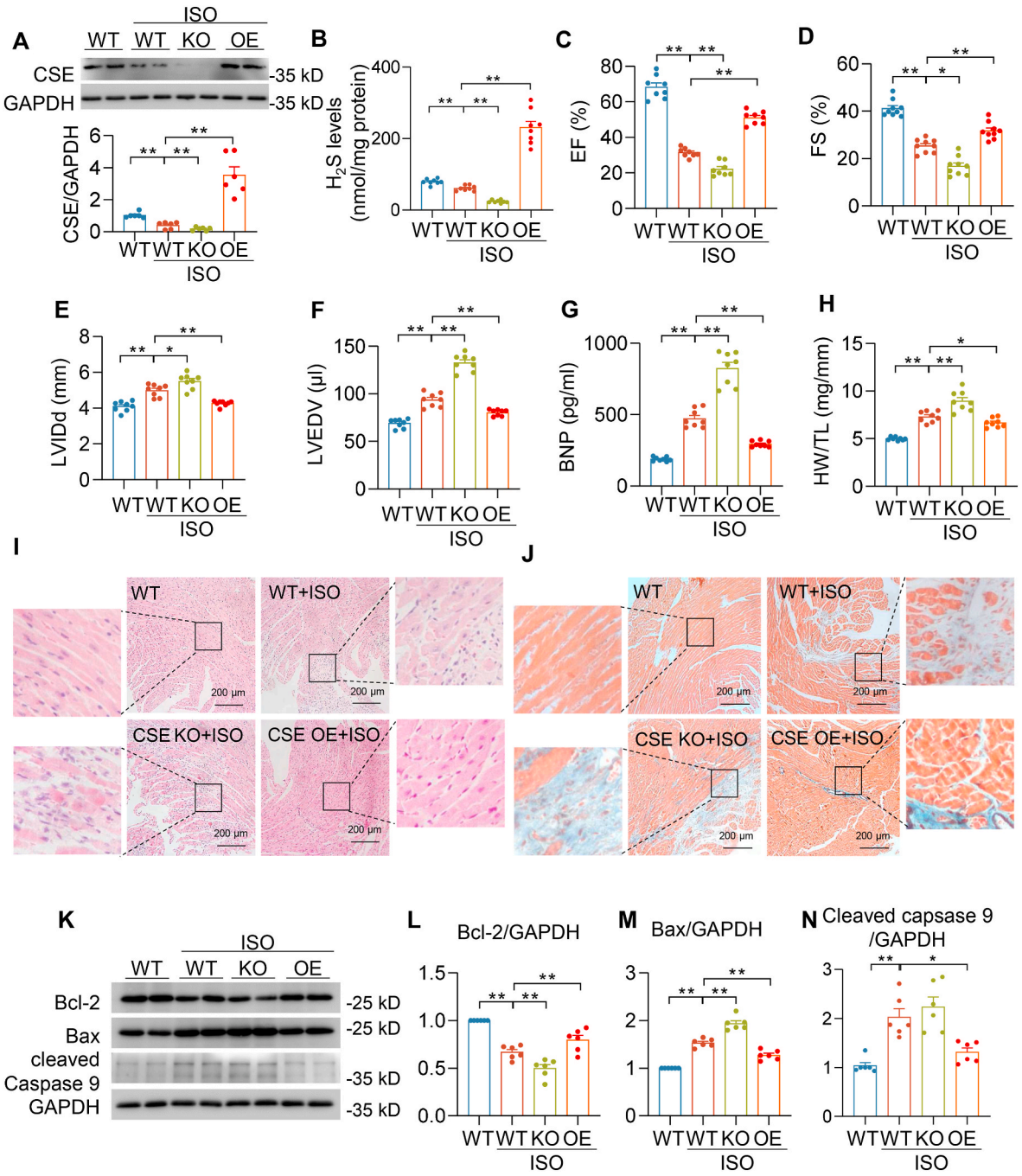


**Fig. 1. CSE/$H_2S$ pathway mediated ISO-induced heart dysfunction.** A, Western blots and summarized data showing CSE protein levels in the indicated hearts of mice injected by vehicle or ISO for 4 weeks. n = 6. B, $H_2S$ concentrations in the indicated hearts of mice injected by vehicle or ISO for 4 weeks. n = 8. C-D, Left ventricular ejection fraction (EF) (C) and left ventricular fraction shortening (FS) were measured by echocardiography (D). n = 8–9. E-F, Left Ventricular internal dimension diastole (E) and left ventricular end-diastolic volume (F) were measured by echocardiography. n = 8. G, Plasma BNP levels in mice after 4 weeks' vehicle or ISO administration. n = 8. H, Quantification of heart weight (HW) over tibia length (TL) ratio in mice injected by vehicle or ISO for 4 weeks. n = 8. I-J, Representative images of HE images (I) and masson trichrome staining images (J) in indicated hearts of mice after 4 weeks' vehicle or ISO administration. Scale bar = 200 μm. K–N, Western blotting images (K) and quantification of Bcl-2 (L), Bax (M) and cleaved caspase 9 (N) protein levels in the indicated hearts of mice after 4 weeks' vehicle or ISO administration. n = 6. *: $p < 0.05$, **: $p < 0.01$.

Beads (Biolinkedin, Cat. No. IK-1004) were added and incubated at room temperature for 2 h. The beads were washed by PBS with 0.1% Triton X-100 for three times. Proteins were eluted by 0.1 mol/L glycine and then subjected to SDS-PAGE for Westernblot.

### 2.12. Confocal imaging

Adult cardiomyocytes were mounted on the confocal microscope (Leica SP8) stage in a custom-made chamber. Cells were immersed in the Tyrode's solution containing KCl (3.1 mmol/L), NaCl (138 mmol/L), $KH_2PO_4$ (1.2 mmol/L), $MgSO_4$ (1.2 mmol/L), $CaCl_2$ (1 mmol/L), HEPES (20 mmol/L) and glucose (5 mmol/L) (pH = 7.4). Cells expressed GFP-Drp1 and GFP-Drp1 C607A for 72 h and co-stained with mitoTracker Red (Invitrogen, Cat No. T668) at room temperature for 20 min. Images were obtained by Leica confocal microscope, tandem excitation at 488 nm and 552 nm, and collecting emissions at 490–530 nm and > 560 nm

respectively. The number and size of GFP dots and mitochondrial size were analyzed by ImageJ software.

The mt-SoNar and mt-cpYFP were monitored in cardiomyocytes on coverslips. Dual-excitation images of mt-SoNar or mt-cpYFP were taken by excitation at 405 nm and 488 nm, and collecting emission at > 505 nm. The NADH/$NAD^+$ ratio was calculated by the fluorescence emission at 405 nm excitation over that of 488 nm excitation for mt-SoNar. The control ratio was analyzed at the same way for mt-cpYFP.

### 2.13. mPTP opening analysis in cardiomyocytes

The mPTP opening was determined by the abrupt loss of membrane potential as previously described [27]. In brief, cardiomyocytes were stained with tetramethylrhodamine, methyl ester (TMRM) (Invitrogen, Cat No. T668, 20 nmol/L) in KHB at 37 °C for 20 min. Confocal linescan was set-up along the long axis of the cardiomyocytes. 10–15 mitochondria showed the clear pattern and were encompassed. TMRM was excited at 552 nm and the emission collected at > 560 nm. The scan speed was at 35 ms per line and the loss of membrane potential was determined by the abrupt decrease in TMRM signal from individual mitochondrion. A shorter mPTP time reports that the pore is more sensitive to the laser-induced opening.

### 2.14. Cell viability assay

Adult cardiomyocytes were incubated with 0.04% trypan blue for 3 min at room temperature. > 80 cardiomyocytes were calculated in 5 randomly images from each sample.

### 2.15. In vitro Drp1 protein expression and purification

For bacterial expression, Drp1 was synthesized and cloned into BamHI between HindIII sites of the pRSETA vector (Thermo Fisher), which includes 6 x His-tag sequence. *Escherichia coli* BL21 (DE3) plysS (Transgene, Cat No. CD701-02) cells were used for the prokaryotic expression of Drp1 protein. Cells were grown in Luria-Bertani (LB) media containing 100 μg/ml ampicillin at 37 °C until the $OD_{600}$ of cell density was 0.5. 0.1 mmol/L isopropyl 1-thio-β-D-galactopyranoside was added to induce protein expression and the temperature was shifted to 4 °C for 7 days. Bacteria were harvested, suspended in 50 mmol/L potassium phosphate buffer (pH = 7.4) and lysed via ultrasonication. After centrifuged at 12,000 rpm for 30 min at 4 °C, the His-tagged Drp1 was purified by Nickle resin (Ni Sepharose 6 Fast Flow, GE Healthcare) followed by 300 mmol/L imidazole elution, desalted and exchanged into 100 mmol/L HEPES buffer with Sephadex column. Drp1 protein was diluted to the required concentration before assay.

### 2.16. RNA extraction and quantitative real-time PCR

Total RNA was extracted from left ventricle tissue using the RNAeasy Extraction Kit (Beyotime, Cat No. R0026) according to the manufacturer's instructions. Total RNA was reversed transcribed to cDNA using the Evo M-MLV Reverse Transcription Kit (Accurate Biology, Cat No. AG11706). cDNA transcripts were quantified by QuantStudio 3 Real-Time PCR System (Thermo Fisher) using SYBR Green (Accurate Biology, Cat No. AG11718). The BNP mRNA level was normalized to the 18S rRNA level and showed as fold-change over control. The primer sequence information is as follows:

BNP, forward: AGCTGCTGGAGCTGATAAGAGAA.
BNP, reverse: GTGAGGCCTTGGTCCTTCAA.
18S, forward: GTAACCCGTTGAACCCCATT.
18S, reverse: CCATCCAATCGGTAGTAGCG.

### 2.17. Biochemical analysis

The GTPase activity in hearts and adult cardiomyocytes was measured after anti-Drp1 antibody pulldown by a GTPase assay kit (Innova Biosciences, Cat. No. 602-0120). The GTP hydrolysis activity was determined at the absorbance at 635 nm by a microplate reader. Plasma brain natriuretic peptide (BNP) levels, NO and ATP concentrations in the heart were measured by using commercial kits (MyBioSource, Cat. No. MBS2510603 for BNP, Beyotime, Cat. No. S0021S for NO, and MilliporeSigma, Cat. No. FLAA for ATP).

### 2.18. Statistical analysis

Statistical analysis was done using analysis of variance (ANOVA or Student's test). Post hoc pairwise comparisons were performed using GraphPad Prism 8.3.0 software. All the data were presented as means ± SEM. A p value $< 0.05$ was considered statistically significant.

## 3. Results

### 3.1. The critical role of CSE/$H_2S$ pathway in heart failure

To precisely evaluate the regulatory role of endogenous $H_2S$ in heart failure, we used CSE knockout (CSE KO) mice and cardiac CSE overexpression (CSE OE) mice. Compared with wild type (WT) mice, no band was observation in the CSE KO mice indicating a complete deletion of CSE protein in the heart. By contrast, the CSE level was significantly elevated (~3 fold) in the CSE OE heart (Fig. S1A). After 4-week isoprenaline (ISO) subcutaneous injection, compared with wild type mice with vehicle treatment (WT-Con), CSE protein levels and $H_2S$ concentrations were obviously decreased in wild type mice with ISO treatment (WT-ISO). In line with CSE protein levels, the $H_2S$ concentration was lowest in the CSE KO–ISO mice and substantially increased in CSE OE-ISO mice (Fig. 1A–B). Our previous data reported that compared with WT mice, ejection fraction, fraction shortening, left ventricular anterior wall systole and left ventricular posterior wall systole were moderate declined in CSE KO mice [21], which was due to CSE depletion-induced hypertension [28]. ISO rendered more severe heart failure in CSE KO when compared with ISO-induced heart dysfunction in WT mice [21]. However, an exogenous $H_2S$ donor could rescue the heart function in CSE KO mice that indicating $H_2S$ played a critical role in the regulation of cardiac function [21]. Here, echocardiography revealed that CSE deficiency exacerbated ISO-induced decline in ejection fraction and fraction shortening, increase in left ventricular internal dimension diastole and left ventricular end-diastolic volume, which were attenuated in CSE OE-ISO mice (Fig. 1C–F). In addition, compared with WT-ISO mice, CSE KO–ISO mice developed much more severe cardiac hypertrophy, evidenced by brain natriuretic peptide (BNP) levels and heart weight-to-tibia length ratio. Nevertheless, these hypertrophy biomarker levels were significantly abrogated in CSE OE-ISO mice (Fig. 1G–H). Moreover, histological analysis showed the loss of myocardium and increase in fibrosis in CSE KO–ISO hearts. Conversely, no significant changes in these measures were observed in CSE OE-ISO hearts (Fig. 1I–J and Fig. S1B). These results were also consistent with immunoblot showing apoptosis biomarkers (Bcl-2, Bax and cleaved caspapse-9) increased in CSE KO–ISO hearts and decreased in CSE OE-ISO hearts (Fig. 1K-N). Taken together, these findings suggested CSE/$H_2S$ pathway mediated the development of cardiac dysfunction and pathological remodeling of the heart in mice during chronic β adrenergic receptor activation.

### 3.2. $H_2S$ regulated Drp1 activity in heart failure

Mitochondrial morphology, associated with cardiac function, is a pathogenic hallmark of cardiomyopathy [9,10,29]. We performed electron microscopy (EM) analysis to examine cardiac ultrastructure in WT, CSE KO and CSE OE mice with vehicle or ISO treatment. EM images showed that mitochondrion size was decreased in WT-ISO heart, consistent with previous reports that demonstrated an association

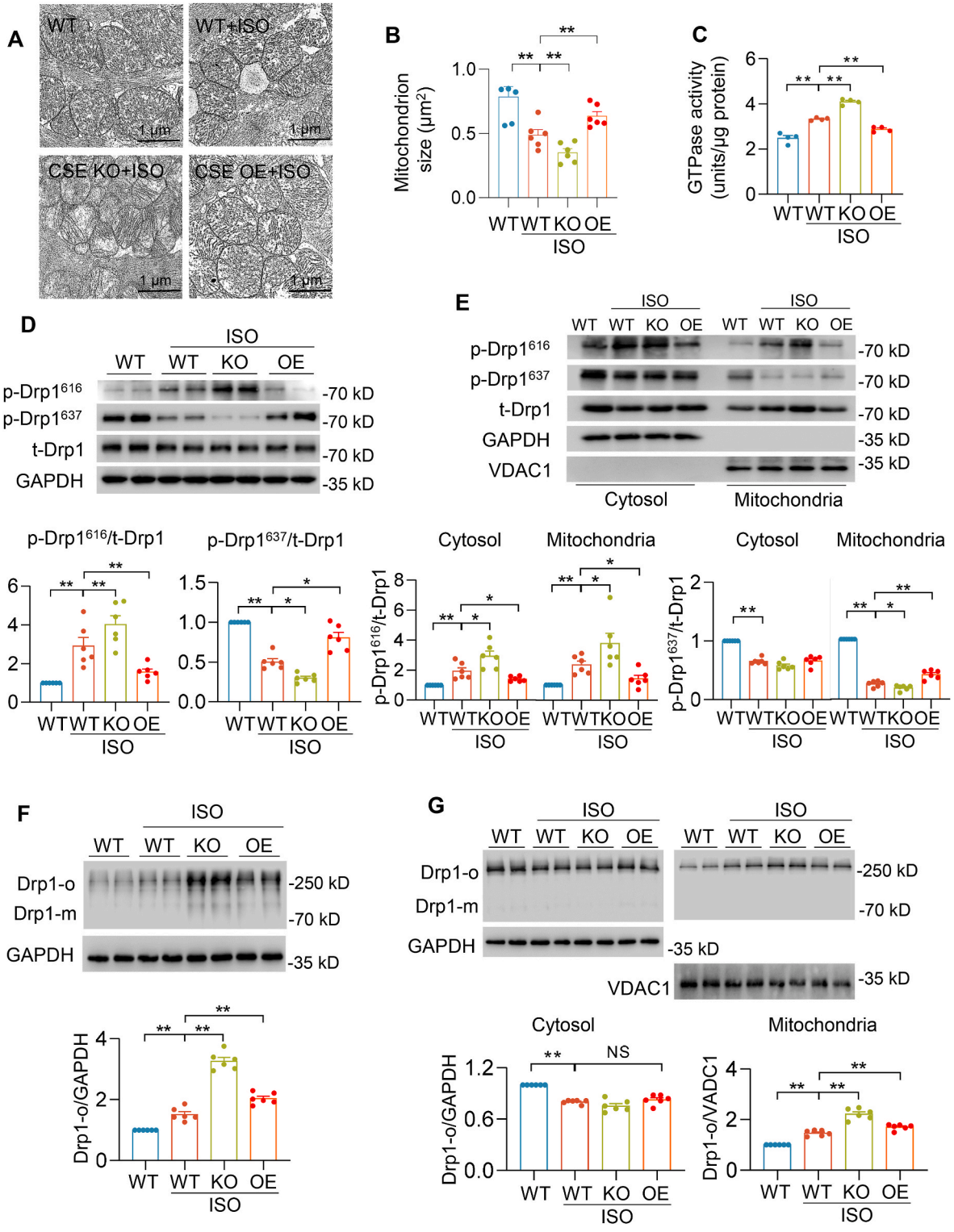


**Fig. 2. CSE/$H_2S$ pathway regulated Drp1 activity in ISO-induced heart failure.** A-B, Electron microscopic images (A) and quantification of mitochondrion size (B) in the indicated hearts of mice after 4 weeks' vehicle or ISO administration. Scale bar = 2 μm n = 210–350 mitochondria from 6 mice for each group. C, The GTPase activity of Drp1 in the indicated hearts of mice after 4 weeks' vehicle or ISO administration. n = 4. D, Western blotting images and quantification of Drp1 phosphorylation at S616 (p-Drp1$^{616}$) and S637 (p-Drp1$^{637}$) levels in the indicated hearts of mice after 4 weeks' vehicle or ISO administration. n = 6. E, Western blotting images and quantification of Drp1 phosphorylation at S616 (p-Drp1$^{616}$) and S637 (p-Drp1$^{637}$) levels in the cytosolic or mitochondrial fraction from the indicated hearts of mice after 4 weeks' vehicle or ISO administration. n = 6. F-G, Western blotting images and summarized data showing Drp1 oligomerization in whole heart (F), cytosolic or mitochondrial fraction (G) from mice after 4 weeks' vehicle or ISO administration. *: $p < 0.05$, **: $p < 0.01$.

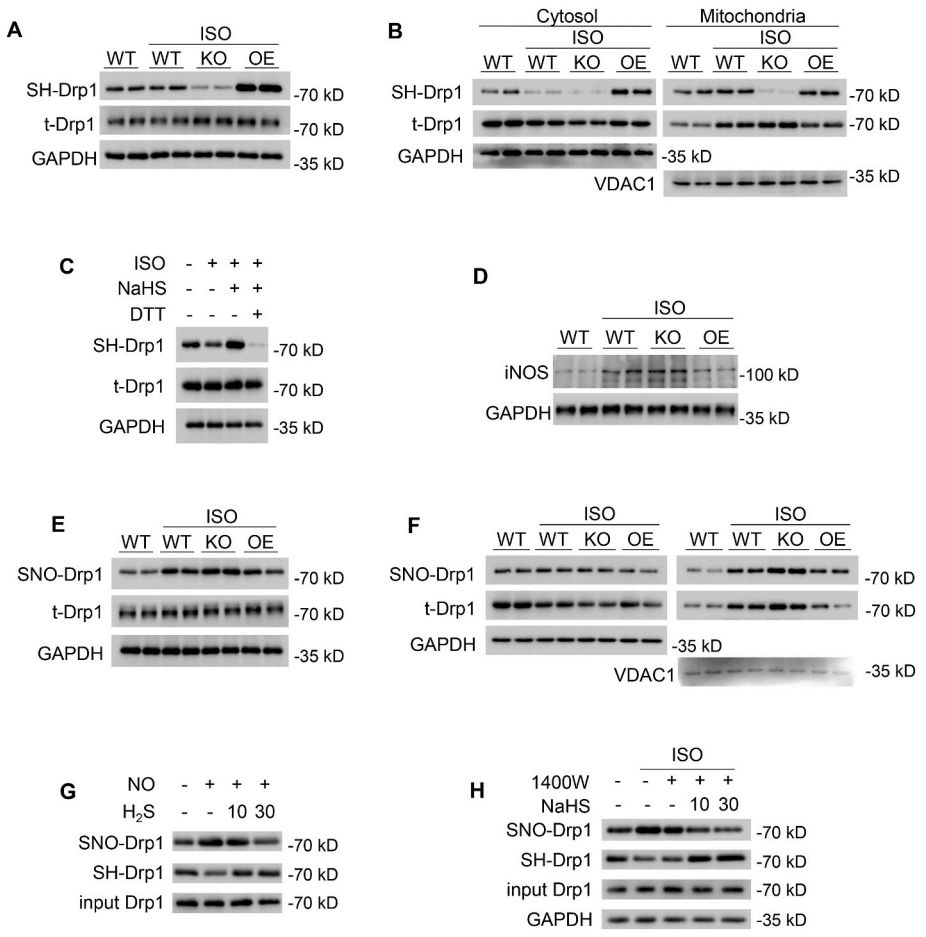


**Fig. 3. $H_2S$ S-sulfhydrated Drp1 and modulated Drp1 S-nitrosylation in heart failure.** A-B, Western blotting images showing Drp1 S-sulfhydration levels in whole heart (A), cytosolic or mitochondrial fraction (B) from mice after 4 weeks' vehicle or ISO administration. n = 6. C, Western blotting images showing Drp1 S-sulfhydration levels in adult cardiomyocytes incubated with or without ISO (1 μmol/L, 48 h), NaHS (30 μmol/L, 48 h) and DTT (1 mmol/L, 1 h). n = 6. D, Western blotting images showing iNOS protein levels in the indicated hearts of mice after 4 weeks' vehicle or ISO administration. n = 6. E-F, Western blotting images showing Drp1 S-nitrosylation levels in whole heart (E), cytosolic or mitochondrial fraction (F) from mice after 4 weeks' vehicle or ISO administration. n = 6. G, Western blotting images showing Drp1 S-sulfhydration and S-nitrosylation *in vitro* incubated with SNP (10 μmol/L) or/and NaHS (10 μmol/Lor 30 μmol/L). n = 6. H, Western blotting images showing Drp1 S-sulfhydration and S-nitrosylation in adult cardiomyocytes with 1400W (200 μmol/L) or/and NaHS (10 μmol/Lor 30 μmol/L) after ISO treatment. n = 6. *: $p < 0.05$, **: $p < 0.01$.

between heart failure and mitochondrial morphology [10]. Furthermore, CSE KO–ISO heart showed much smaller mitochondrion size compared with that in WT-ISO heart. However, the mitochondrion size was preserved in CSE OE-ISO heart (Fig. 2A–B). These results indicated that $H_2S$ have a critical role in regulation of mitochondria fission. To investigate the mitochondrial morphological changes, we determined the Drp1 activity and protein level. The basal GTP-hydrolyzing activity of Drp1 was modestly increased or decreased in CSE KO or OE hearts respectively when compares with WT hearts (Fig. S2A). Furthermore, GTP-hydrolyzing activity of Drp1 was enhanced in CSE KO–ISO hearts and reduced in CSE OE-ISO hearts compared with WT-ISO hearts (Fig. 2C). Immunoblot analysis showed that ISO did not lead to increase the total Drp1 protein level in all hearts (Fig. S2B), but increased Drp1 protein levels were mainly found in the mitochondrial fraction from WT-ISO heart. Interestingly, compared with WT-ISO hearts, mitochondrial Drp1 levels were much more in CSE KO–ISO hearts, which were normalized in CSE OE-ISO hearts (Fig. 2D–E, and S2C-D). Drp1 translocation from cytosol to mitochondria is regulated by various signals and post-translational modifications. Phosphorylation of Drp1 at serine 616 (S616) promotes its translocation, while Drp1 phosphorylation at serine 637 (S637) is inhibitory [30]. We observed that ISO increased the phosphorylation of Drp1 at S616, but decreased Drp1 phosphorylation at S637 in WT-ISO heart, cytosolic and mitochondrial fractions. Moreover, higher Drp1 phosphorylation at S616 and lower Drp1 phosphorylation at S637 were obtained in CSE KO–ISO hearts. Conversely, these changes were attenuated in CSE OE-ISO hearts (Fig. 2D–E). Next, we used native PAGE gel to investigate Drp1 oligomers indicating Drp1 activity. Drp1 oligomers were increased in WT-ISO and CSE KO–ISO hearts and mitochondrial fraction. By contrast, CSE OE-ISO hearts and mitochondrial fraction showed that abnormal Drp1 oligomers were alleviated (Fig. 2F–G). In summary, $H_2S$ modulated the phosphorylation, translocation, oligomerization and GTPase activity of Drp1 in heart failure.

### 3.3. $H_2S$ S-sulfhydrated Drp1 via directly competing with S-nitrosylation in the heart

Increasing evidence highlights that S-sulfhydration as a post-translational modification is a major mechanism by which $H_2S$ exerts physiological influence [31,32]. Firstly, we assessed the total S-sulfhydration in the heart. The whole-heart homogenates were subjected to the biotin-switch assay, the captured proteins were resolved by SDS-PAGE and gels were Coomassie blue stained. Compared with the WT heart, the total S-sulfhydration level was decreased in the CSE KO heart, but increased in the CSE OE heart. It suggested that CSE is a critical regulator of S-sulfhydration level in the heart (Fig. S3A). Furthermore, the biotin-switch analysis revealed that Drp1 S-sulfhydration level was notably decreased in WT-ISO hearts and mitochondria fraction. In addition, CSE deficiency further downregulated Drp1 S-sulfhydration level, whereas CSE overexpressing potentiated Drp1 S-sulfhydration level either in whole heart or mitochondria fraction (Fig. 3A–B and Figs. S3B–D). To further determine whether $H_2S$ could directly S-sulfhydrate Drp1, we added dithiothreitol (DTT, 1 mmol/L for 1 h) in adult cardiomyocytes to produce the reduced environment. It was noticed that although $H_2S$ prevented the decline of ISO-induced Drp1 S-sulfhydration, S-sulfhydration of Drp1 was substantial abrogated by DTT treatment, which indicating the liberation of –SH group from the key cysteine residue (Fig. 3C and Fig. S3E).

Previous studies have shown that nitric oxide (NO) also post-modified Drp1 as S-nitrosylation which promoted mitochondrial

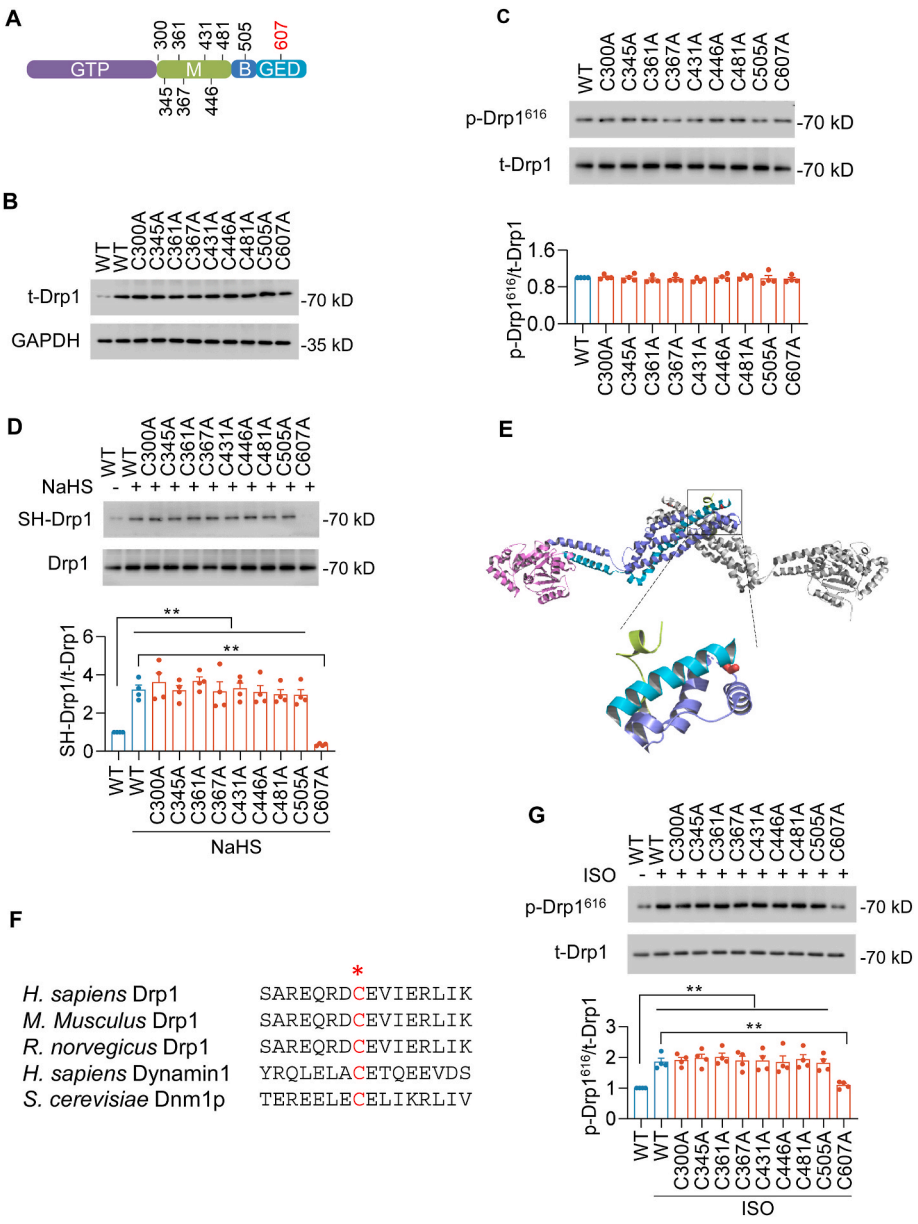


**Fig. 4. S-sulfhydration of Drp1 was determined at cysteine 607.** A, Scheme showing the locations of 9 cystine residues in Drp1 that can be S-sulfhydrated. The domains are GTPase domain (GTP), middle domain (M), B domain (B), and GTPase effector domain (GED). B, Western blotting images showing expression levels of wild-type (WT) and mutations of Drp1 48 h after gene transfer in HEK293 cells. C, Western blotting images and summarized data showing the phosphorylation at S616 (p-Drp1$^{616}$) of WT and mutations of Drp1 48 h after gene transfer in HEK293 cells in the absence of ISO or NaHS. n = 4. D, Western blotting images and summarized data showing the S-Sulfhydration of Drp1 and its mutants in HEK293 cells incubation with NaHS (30 μmol/L, 48 h). n = 4. E, Homology modeling of human Drp1 (PDB:4BEJ) shows cysteine 607 (red) is exposure out of Drp1 protein and cysteine 607 is in the soft location of α helix terminal. F, Comparison of Drp1 sequences in the GED domains among different Drp1 homologous. *H. sapiens* Drp1 600–615, *M. musculus* Drp1 624–639, *R. norvegicus* Drp1 617–632, *H. sapiens* Dynamin1 597–612, *S. cerevisiae* Dnm1p 663–678. The cysteine 607 in Drp1 sequences (red) is highly conserved among different species. G, Western blotting images and summarized data showing the effects of WT or mutants on ISO-induced Drp1 phosphorylation at S616. n = 4. **: $p < 0.01$. (For interpretation of the references to colour in this figure legend, the reader is referred to the Web version of this article.)

fission [33], but the regulatory relationship between S-nitrosylation and S-sulfhydration of Drp1 remains unknown. Firstly, we examined the inducible nitric oxide synthase (iNOS) protein levels and NO concentrations in the heart. We found that both iNOS protein levels and NO concentrations were significantly augmented in WT-ISO and CSE KO–ISO hearts, whereas they were alleviated in CSE OE-ISO hearts (Fig. 3D, Figs. S3F–G). These data suggested that $H_2S$ mediated iNOS/NO pathway. Consistently, the WT-ISO hearts and mitochondria fraction showed S-nitrosylation of Drp1 was potentiated. When compared with the WT-ISO heart, the level of Drp1 S-nitrosylation was increased more in CSE KO–ISO hearts and mitochondria fraction. However, the altered Drp1 S-nitrosylation was abrogated in CSE OE-ISO hearts and mitochondria fraction (Fig. 3E–F and Figs. S3H–J). These findings revealed that $H_2S$ directly S-sulfhydrated Drp1 and affected Drp1 S-nitrosylation. To identify whether $H_2S$ directly competed with NO or via iNOS pathway to modify Drp1, purified Drp1 protein was incubated with sodium nitroprusside (10 μmol/L SNP, a NO donor) or/and NaHS for 1 h. SNP significantly increased SNO-Drp1 level, however NaHS (10 or 30 μmol/L) does-dependently decreased SNO-Drp1 level and potentiated Drp1 S-sulfhydration level (Fig. 3G and Fig. S3K-L). These data indicated that $H_2S$ still S-sulfhydrated Drp1 in the absence of iNOS. To further confirm $H_2S$ directly competed with SNO-Drp1 in cardiomyocytes, an iNOS specific inhibitor, 1400W (200 μmol/L), was pretreated cardiomyocytes to inhibit iNOS activity. $H_2S$ still does-dependently decreased SNO-Drp1 level and potentiated Drp1 S-sulfhydration level, although iNOS activity was prevented by 1400W (Fig. 3H and Figs. S3M–N). Taken together, these results suggested that $H_2S$ directly competed with NO to modify Drp1 (Fig. S3O).

### 3.4. Identification of the cysteine residue in Drp1 that was S-sulfhydrated

We next sought to further examine the target cysteine residue for S-sulfhydration on Drp1. Sequence alignment revealed that Drp1 has four distinct domains including an N-terminal guanosine triphosphatase (GTPase) domain, a dynamin-like middle domain, a B domain and a GTPase effector domain (GED). In search of S-sulfhydrated cysteine residue, we mutated each of nine Drp1 cysteines (cysteine (C) to alanine (A), which mimics a non-sulfhydrated state without altering the amino acid structure) (Fig. 4A). After transfection in HEK293 cells, WT and mutations of Drp1 had the similar protein expression levels and

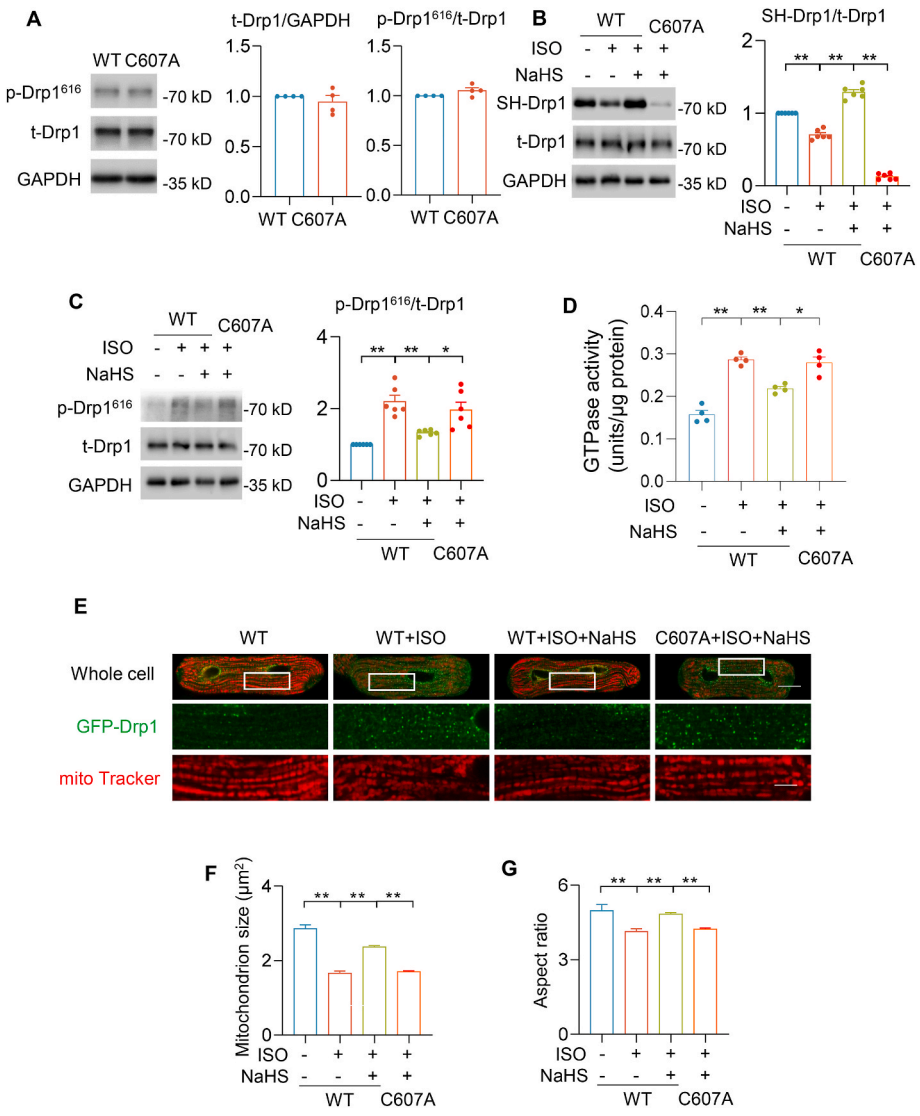


**Fig. 5. Drp1 S-sulfhydration at cysteine 607 regulated its activity and mitochondrial fission.** A, Western blotting images and summarized data showing the Drp1 protein levels and phosphorylation at S616 (p-Drp1616) of Drp1 WT and C607A 72 h after adenovirus-mediated gene transfer in adult cardiomyocytes in the absence of ISO or NaHS. n = 4. B-G, Ad-Drp1 WT and Ad-Drp1 C607A respectively infected adult cardiomyocytes for 24 h. ISO (1 μmol/L) with or without NaHS (30 μmol/L) was added to cardiomyocytes and incubated for 48 h. Western blotting images and summarized data showing the S-sulfhydration level (B) and phosphorylation (C) of Ad-Drp1 WT and Ad-Drp1 C607A mutation in adult cardiomyocytes after ISO and NaHS treatments. The GTPase activity of Drp1 in adult cardiomyocytes overexpressing Ad-Drp1 WT or C607A after ISO and NaHS treatments (D). N = 4. Representative confocal images and summarized data showing mitochondrial size in adult cardiomyocytes overexpressing Ad-GFP-Drp1 WT or C607A after ISO and NaHS treatments (E–G). n = 262–409 mitochondria or 4255–7390 GFP puncta in 20–27 cells from 3 to 4 rats in each group. Scale bar = 20 or 5 μm for the whole cell or enlarged images, respectively.

phosphorylation levels, suggesting that C-to-A mutations did not change Drp1 activity (Fig. 4B–C and S4A). Biotin-switch assay suggested that NaHS (30 μmol/L for 48 h) potentiated S-sulfhydration of WT Drp1 and most of the point mutations, except C607A, indicating C607 was the S-sulfhydrated residue (Fig. 4D). In the 3D structure of Drp1, C607 is a surface residue and accessible for S-sulfhydration (Fig. 4E). Furthermore, the C607 locates at the terminal of α helix that connects the soft linker. In addition, C607 is highly conserved among GED domain cross different species, indicating it is a key residue for Drp1 activation through regulating its structure conformation (Fig. 4F). To test this hypothesis, we determined changes in Drp1 phosphorylation. Upon ISO incubation, Drp1 phosphorylation levels were potentiated in Drp1 WT and most of Drp1 mutations transduced cells. However, Drp1 C607A abrogated the increase in Drp1 phosphorylation levels (Fig. 4G). Taken together, these experiments demonstrate that C607 is specifically S-sulfhydrated and is a critical residue for Drp1 activation.

### 3.5. *C607A mutation blocked Drp1 S-sulfhydration and activity in cardiomyocytes*

To further demonstrate Drp1 S-sulfhydration at cysteine 607 plays a critical role in modulating its activity and function, we constructed adenoviruses containing Drp1 WT (Ad-Drp1 WT) and Drp1 C607A (Ad-Drp1 C607A), and infected adult cardiomyocytes. Drp1 expression and phosphorylation at S616 were comparable between WT and C607A mutation, suggesting that C-to-A mutation did not alter Drp1 basic features (Fig. 5A). Next, we tested whether $H_2S$ S-sulfhydrated Drp1 at the specific residue C607 during ISO-induced mitochondrial fission in cardiomyocytes. NaHS (30 μmol/L for 48 h) was added into Ad-Drp1 WT or Ad-Drp1 C607A overexpressing cardiomyocytes, which were incubated with or without ISO (1 μmol/L) for 48 h. We noticed that ISO incubation decreased S-sulfhydration of Drp1. Although cardiomyocytes were incubation with NaHS, the S-sulfhydration level was hardly observation in Ad-Drp1 C607A-overexpressing cardiomyocytes (Fig. 5B). Furthermore, both phosphorylation at S616 and GTPase activity of Drp1 were augmented by ISO treatment in Ad-Drp1 WT overexpression cardiomyocytes (Fig. 5C–D). NaHS incubation abrogated ISO-induced abnormal Drp1 activity. However, the restored activity was not observed in Ad-Drp1 C607A-overexpressing cardiomyocytes with NaHS treatment (Fig. 5C–D). To further investigate mitochondrial morphology, we constructed adenovirus containing GFP-Drp1 WT (Ad-GFP-Drp1 WT) and GFP-Drp1 C607A (Ad-GFP-Drp1 C607A). In addition, confocal images showed that ISO incubation accelerated mitochondria fission in adult cardiomyocytes, which was alleviated by NaHS treatment. However, NaHS incubation did not abrogate ISO-induced mitochondria fission in Ad-GFP-Drp1 C607A-overexpressing adult cardiomyocytes (Fig. 5E–G). Taken together, these results suggested that $H_2S$ S-sulfhydrated Drp1 at the specific cysteine 607 that regulated its

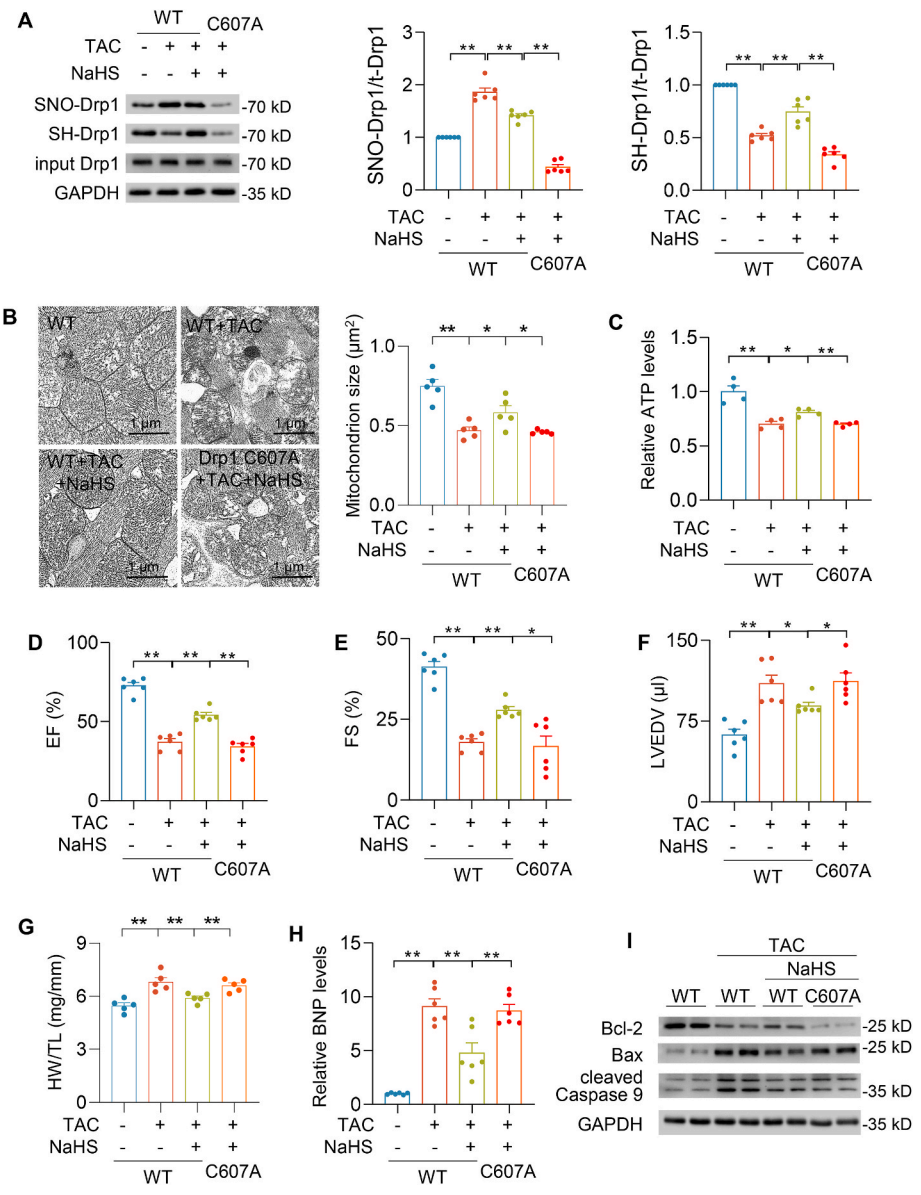


**Fig. 6.** Drp1 S-sulfhydration protected against TAC-induced heart failure

A-I, Purified Drp1 WT and Drp1 C607A adenovirus ($1 \times 10^9$ opu) were respectively administered by direct injection to the LV free wall (three sites, 25 μl/site) of mice. TAC surgery and NaHS (60 μmol/kg/day) intraperitoneal injection were performed 5 days after injection. Western blotting images and summarized data showing Drp1 S-sulfhydration and S-nitrosylation levels after pressure overload generated by TAC for 4 weeks (A). n = 6. Electron microscopic images and quantification of mitochondrion size in the indicated hearts of mice after pressure overload generated by TAC for 4 weeks (B). Scale bar = 2 μm n = 687–907 mitochondria from 5 mice for each group. The ATP level measurements in the heart after pressure overload generated by TAC for 4 weeks (C). n = 6. Left ventricular ejection fraction (D), fraction shortening (E) and left ventricular end-diastolic volume (F) were measured by echocardiography after pressure overload generated by TAC for 4 weeks. n = 6. Quantification of heart weight (HW) over tibia length (TL) ratio in mice after pressure overload generated by TAC for 4 weeks (G). n = 6. qRT-PCR analyses of BNP genes in the heart after pressure overload generated by TAC for 4 weeks. The expression was normalized to 18S rRNA and reported as fold change over WT (H). Western blotting images of Bcl-2, Bax and cleaved caspase 9 protein levels in the indicated hearts of mice after pressure overload generated by TAC for 4 weeks (I). *: $p < 0.05$, **: $p < 0.01$.

activity and function in adult cardiomyocytes.

### 3.6. *Drp1 C607A mutation abrogated the protective effect of $H_2S$ against heart failure*

To further determine the regulatory effect of $H_2S$ on Drp1 S-sulfhydration *in vivo*, mouse heart failure model was constructed by transverse aortic constriction (TAC) and Drp1 WT and Drp1 C607A proteins were overexpressed in the heart by adenovirus injection *in situ*. The efficacy of adenovirus injection was confirmed by immunoblot (Fig. S6A). After TAC for 4 weeks, Drp1 S-sulfhydration and S-nitrosylation levels were significantly decreased and increased respectively. NaHS (60 μmol/kg/day for 4 weeks) intraperitoneal administration potentiated the Drp1 S-sulfhydration level and abrogated Drp1 S-nitrosylation. By contrast, neither S-sulfhydration nor S-nitrosylation of Drp1 was observed in Drp1 C607A-overexpressing hearts (Fig. 6A). NaHS prevented TAC rendered mitochondrial hyperfission in WT-TAC-NaHS hearts, not in Drp1 C607A-TAC-NaHS hearts (Fig. 6B). In line with Drp1 S-sulfhydration and mitochondria size, TAC injured mitochondrial energy metabolism, but ATP production was also elevated by NaHS in WT-overexpresing hearts, but not in Drp1 C607A-expressing hearts (Fig. 6C). Compared with WT-Con hearts, TAC caused significant cardiac dysfunction, heart hypertrophy, increased BNP level and apoptosis biomarkers in WT-TAC hearts (Fig. 6D–I and Figs. S6B–D). NaHS alleviated TAC-induced heart hypertrophy and the increase of BNP level, which were not observed in Drp1 C607A-TAC-NaHS hearts (Fig. 6D–I). Furthermore, NaHS ameliorated TAC caused decline in ejection fraction, fraction shortening and increase in left ventricular end-diastolic volume. Conversely, Drp1 C607A overexpression suppressed the protective role of $H_2S$ in Drp1 C607A-TAC-NaHS hearts (Fig. 6D–I). In summary, the data strongly supported the Drp1 at cysteine 607 was a critical residue for S-sulfhydration by $H_2S$, which alleviated abnormal mitochondrial fission and the development of heart failure in mice.

### 3.7. *S-sulfhydration of Drp1 reduced interaction with VDAC1 to maintain cardiomyocyte function*

To study how Drp1 S-sulfhydration protects against heart dysfunction, we performed co-immunoprecipitation and found that Drp1 interacted with Voltage-dependent anion channel 1 (VDAC1), which regulates mitochondria function and cell apoptosis [34,35]. ISO potentiated the interaction between Drp1 and VDAC1 in the heart. Moreover,

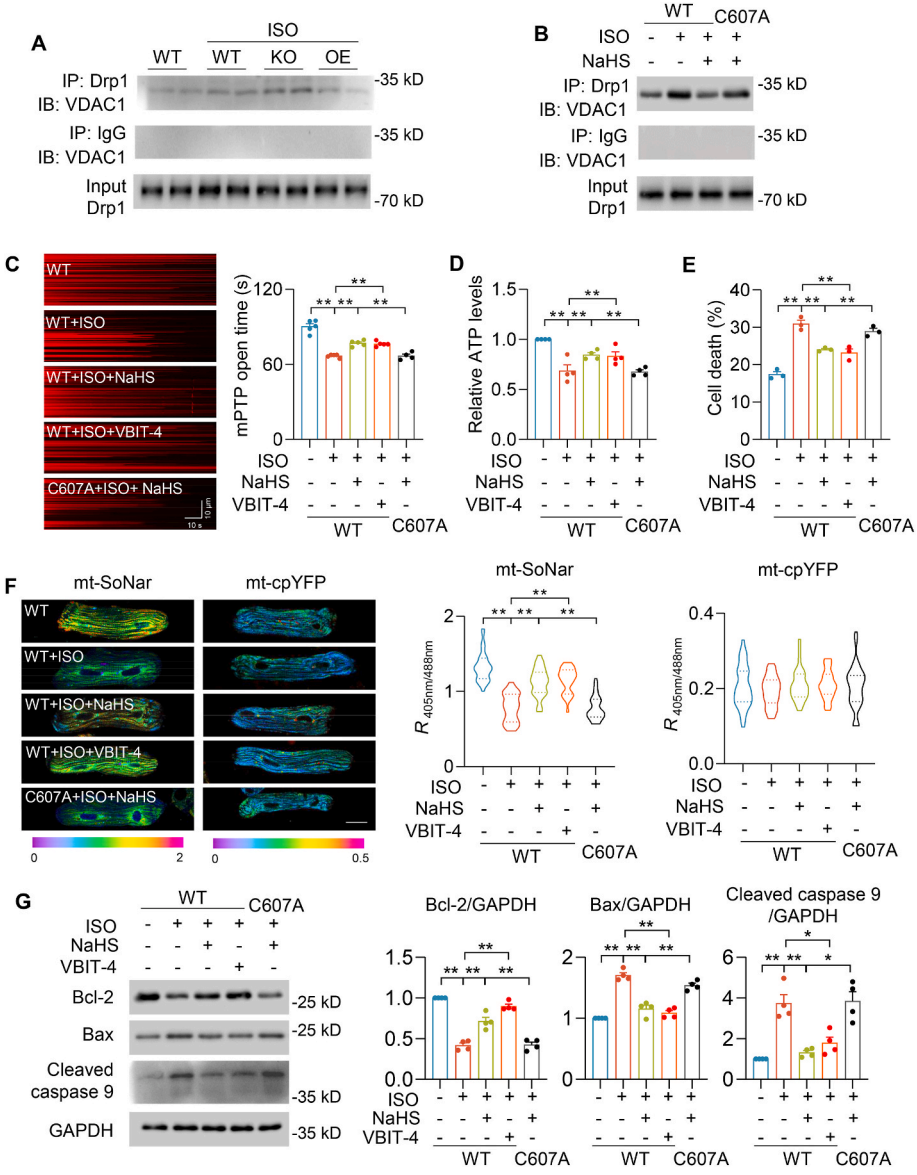


**Fig. 7. S-sulfhydration at cysteine 607 prevented Drp1 and VDAC1 interaction and regulated ISO-induced mitochondrial dysfunction.** A, Western blots showing Drp1 and VDAC1 interactions in the indicated hearts of mice after 4 weeks' vehicle or ISO administration. B, Western blots showing the interactions between Drp1 WT and VDAC1 or Drp1 C607A and VDAC1 in the adult cardiomyocytes incubated with or without ISO (1 μmol/L, 48 h) and NaHS (30 μmol/L, 48 h). C, Representative linescan confocal images and summarized data showing the laser-induced permanent loss of $\Delta\psi_m$ in individual mitochondrion. n = 547–900 mitochondria in 31–37 cells from 4 to 5 rats in each group. D-E, Effects of ISO (1 μmol/L, 48 h) on ATP levels (D), and cell death (E) in adult cardiomyocytes with or without overexpression of Drp1 WT or C607A, or pretreatment of VBIT-4 (10 μmol/L, 48 h). n = 3–4. F, Representative fluorescence images and quantification of mt-SoNar or mt-cpYFP in adult cardiomyocytes expressed Drp1 WT or C607A with or without ISO (1 μmol/L, 48 h), NaHS (30 μmol/L, 48 h) or VBIT-4 (10 μmol/L, 48 h). n = 29–34 cells from 3 rats in each group. Scale bar = 20 μm. G, Western blots images and summarized data showing effects of ISO on Bcl-2, Bax and cleaved caspase 9 in adult cardiomyocytes and with overexpression of Drp1 WT or C607A or pretreatment of VBIT-4. n = 4. *: $p < 0.05$, **: $p < 0.01$.

this interaction was further augmented in CSE KO–ISO hearts, which was prevented in CSE OE-ISO hearts (Fig. 7A and S7A). In cultured adult cardiomyocytes, ISO also enhanced the interaction between Drp1 WT and VDAC1, but not between Drp1 C607A and VDAC1 (Fig. 7AB and S7B). These results indicated that Drp1 binding with VDAC1 was modulated by S-sulfhydration modification. Either $H_2S$ or a specific VDAC1 inhibitor (VBIT-4,10 μmol/L for 48 h) [36], blocked ISO-induced mPTP opening and decline in ATP levels in Drp1 WT-expressing adult cardiomyocytes, but these effects were attenuated by overexpression of Drp1 C607A (Fig. 7C–D). Recently we developed a genetic fluorescent indicator, mt-SoNar, to evaluate mitochondrial NADH/$NAD^+$ ratio that is closely linked to mitochondria function [24]. Confocal images showed that ISO decreased mt-SoNar fluorescence, which was prevented by $H_2S$ or VBIT-4 incubation in Drp1 WT, not in C607A, overexpression adult cardiomyocytes. As the control, mt-cpYFP fluorescence did not significantly change upon ISO, $H_2S$, or VBIT-4 treatment in either Drp1 WT or C607A-expressing adult cardiomyocytes (Fig. 7F). Moreover, $H_2S$ or VBIT-4 incubation dramatically prevented ISO-induced cardiomyocyte death with Drp1 WT overexpression, not Drp1 C607A overexpression (Fig. 7E). Immunoblot analysis showed that ISO increased Bcl-2, Bax and caspase 9 cleavage in adult cardiomyocytes, which were abolished by $H_2S$ or VBIT-4 incubation in Drp1 WT, not in C607A, overexpression adult cardiomyocytes (Fig. 7G). In summary, these findings revealed $H_2S$ mediated the interaction between Drp1 and VDAC1, which was an indispensable pathway in ISO-induced mitochondrial dysfunction and cardiomyocyte death.

## 4. Discussion

In this study, we reported a novel post-modification of Drp1 that protects against abnormal mitochondrial fission and heart dysfunction *in vitro* and *in vivo* (Fig. 8). We found that $H_2S$ facilitated S-sulfhydration of the fission protein Drp1, which directly competed with NO-induced Drp1 S-nitrosylation. The S-sulfhydration of Drp1 at cysteine 607 modulated Drp1 phosphorylation, GTPase activity and interaction with VDAC1 to ameliorate mitochondrial dysfunction and cardiomyocyte death. These results are the first to identify that Drp1 S-sulfhydration mediated mitochondrial function in the heart. Based on the findings, interventions leading to restoration of mitochondria morphology by targeting Drp1 S-sulfhydration may offer a potential therapeutic approach for heart failure.

Our study identifies that genetically manipulating CSE/$H_2S$ pathway

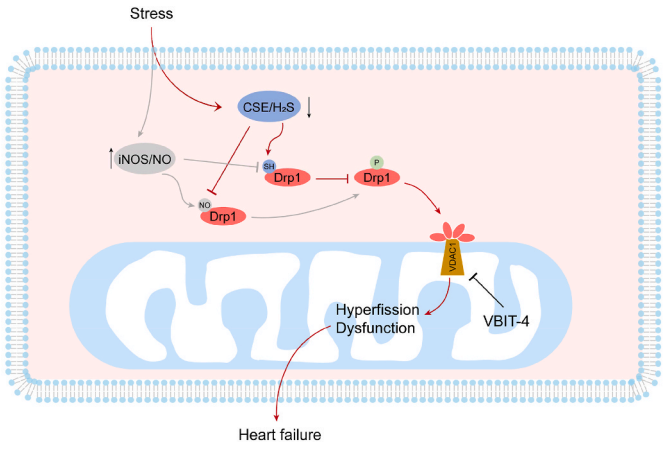


**Fig. 8.** Schematic model showing the mechanism of CSE/$H_2S$ regulated Drp1 activity in heart failure. During heart failure, CSE/$H_2S$ pathway was inhibited, whereas iNOS/NO pathways was potentiated. Although Drp1 S-sulfhydration and S-nitrosylation were competitively modified at the same cysteine, the effect of these two modifications on Drp1 activity was reverse. Aberrant activation of Drp1 translocated to mitochondria outer membrane and interacted with VDAC1 to cause mitochondria hyperfission and dysfunction.

modulated ISO-induced heart function. Activation of β-adrenergic receptor (β-AR) has a critical role in stimulating cardiac output during fight or flight response and chronic β-AR activation contributes to myocardial hypertrophy and heart failure. It is demonstrated that $H_2S$, as an endogenous gasotransmitter, protected against ISO-heart failure. However, previous experiments used $H_2S$-releasing agents or inhibitors to investigate the role of $H_2S$ in heart function [19,21,37]. Increasing evidence reports that $H_2S$ donors released a rapid and largely uncontrollable $H_2S$ and generated various byproducts [16]. L-propargylglycine, as an inhibitor for CSE, has a low potency and cell permeability and is used at very high concentrations [38]. Therefore, we constructed CSE KO or CSE OE mice to precisely evaluate the role of endogenous $H_2S$ in the heart. Our results showed CSE KO mice were more susceptible to chronic ISO stress, whereas heart dysfunction and pathological remodeling were prevented in CSE OE hearts, indicating the essential regulatory of $H_2S$ in the heart function.

Our results also revealed that an important role of Drp1 in the link between $H_2S$ signals and mitochondrial morphology. Mitochondrial morphology is associated to mitochondrial quality control and affects cardiomyocyte function and heart disease development [5]. Ablation of fission proteins in the heart led to mitochondrial dysfunction and heart failure [9,10]. Prior studies by us and other group also found that lipid overload increased Drp1 activity and mitochondrial fission in diabetic cardiomyopathy [11,12]. Although it is known that $H_2S$ plays a central role in mitochondrial homeostasis, the direct evidence for the regulatory effect of $H_2S$ on mitochondrial morphology remains unclear [39]. Drp1 activity potentiated in CSE KO–ISO hears, but it was restored in CSE OE-ISO hearts, which suggesting Drp1 activity was prevented by $H_2S$ to modulate mitochondrial fission. In addition, aberrant mitochondrial fission underlies mitochondrial dysfunction during heart failure. $H_2S$ prevented TAC-induced mitochondrial hyperfission, decline in ATP level and cardiac dysfunction. However, the protective effects of $H_2S$ were abrogated in Drp1 mutant-overexpressing heart. It suggested that the regulation of Drp1 activity would be an important therapy to ameliorate heart failure.

Drp1 activity could be regulated by various post-translational modifications including phosphorylation, acetylation, S-nitrosylation, O-GlucNAcylation, SUMOylation and ubiquitination [7]. The S-sulfhydration of Drp1 at cysteine 607 is a novel post-translational modification. S-sulfhydration is an important signaling pathway of $H_2S$, which exerting its regulatory effects. Nishimura et al. found that Drp1 in neonatal rat cardiomyocytes was polysulfidated at cysteine 624 (cysteine 607 of human Drp1), and depolysulfidation of Cys624-S(n)H in rat Drp1, which led to filamin-dependent activation of Drp1 and mitochondrial hyperfission [40]. Here, we firstly reported that Drp1 S-sulfhydration is required for modulating phosphorylation at S616, and GTPase activity of Drp1. These results indicate that S-sulfhydration at cysteine 607 may initiate sequential steps in Drp1 activation. Blockade of Drp1 S-sulfhydration by site-directed mutagenesis, the protective effect of $H_2S$ was abrogated on heart failure and mitochondrial fission. Therefore, targeting Drp1 S-sulfhydration could prevent Drp1 overactivation and cardiac dysfunction.

It has been shown that Drp1 activity was also regulated by the S-nitrosylation of Drp1, which promoted mitochondrial fission [33]. However, $H_2S$-induced Drp1 S-sulfhydration inhibited mitochondrial fission. These results suggest that Drp1 functions are intricately regulated by redox conditions. Interestingly, Drp1 activity is competitively regulated

by S-sulfhydration and S-nitrosylation at cysteine 607. Our data showed that *in vitro* increased $H_2S$ levels significantly alleviated S-nitrosylaion of Drp1 protein. After blockade of iNOS activity, $H_2S$ still could augmented Drp1 S-sulfhydration by suppressing its S-nitrosylation. ISO decreased both $H_2S$ and Drp1 S-sulfhydration levels in the heart, whereas the NO and Drp1 S-nitrosylation levels were increased. However, the results were adverse in CSE OE hearts. Thus, the competition of –NO and –SH for cysteine residues may be dependent on the relative concentrations.

Either $H_2S$ or NO covalently attaches to the thiol side chain of cysteine residues to form S-sulfhydration or S-nitrosylation respectively. The covalent bond is affected by several factors, such as cell redox environment, metal ions, local pH and so on, which alters thiol reactivity to S-sulfhydration and S-nitrosylation. On one hand, the S-nitrosylated bond is weaker than S-sulfhydrated bond, therefore S-sulfhydrated cysteine is more stable than S-nitrosylated cysteine [25]. $H_2S$ dissociates to hydrosulfide ($HS^-$) at pH 7.4 and reacts with S-nitrosylated cysteine, and then releases NO to produce S-sulfhydrated cysteine. On the other hand, we and other group [40] found Drp1 depolysulfurization in heart failure. The underlying mechanisms are complex. For example, cell redox environment, metal ions or local pH changes may cause Drp1 depolysulfurization. It would be needed to determine which effector plays a critical role in Drp1 depolysulfurization in the future. Moreover, $H_2S$ and NO also competitively regulate non-modified Drp1 protein to govern Drp1 S-sulfhydration or S-nitrosylation levels by their relative concentrations. Therefore, Drp1 post translational modification is a dynamic process. In addition, increasing study reported that CSE used cysteine to generate CysSSH, which could be directly incorporated target protein during translation in cells [41,42]. Although we detected $H_2S$ level associated with CSE expression level, there is a potential molecular pathway that CSE-derived CysSSH may be directly incorporated into Drp1. It is also worthy to investigate the regulatory role of CSE-derived CysSSH on Drp1 activity in the future.

Our study identifies that the non-canonical role of Drp1 interacts with VDAC1 to cause mitochondria dysfunction and cell death. Compelling evidence reports that Drp1 has non-canonical functions, including mitochondrial energetics and mPTP opening [13]. VDAC1 plays an important role in mitochondrial hormesis and cell apoptosis [34,35]. The current study showed that Drp1 S-sulfhydration affects mitochondria function and cardiomyocyte viability through interacting with VDAC1. The inhibition of VDAC1 activity restored ISO-induced mitochondria dysfunction, but the mechanism for this Drp1-VDAC1 interaction remains to be further determined. In addition, how Drp1 S-sulfhydration at cysteine 607 regulates its phosphorylation and activity is also needed to be deeply investigated.

In summary, we demonstrate that CSE/$H_2S$ pathway mediates TAC or ISO-induced cardiac dysfunction and pathological remodeling through regulating Drp1 activity. Furthermore, the findings from the present study indicate that Drp1 S-sulfhydration at cysteine 607

prevents its activity, translocation and interaction with VDAC1 to induce mitochondrial dysfunction and cardiomyocyte death. Targeting Drp1 S-sulfhydration may offer a promising approach to ameliorate the heart failure.

## Source of funding

This work was supported by the Science and Technology Commission of Shanghai Municipality, China (22ZR1456900 to D.W.), National Natural Science Foundation of China, China (82100405 to Q.H., 81703499 to D.W.), Shanghai Pujiang Program, China (2020PJD055 to D.W.), Shanghai Chenguang Program, China (17CG13 to D.W.).

## Author contributions

Q.H. conceived the concept. Q.H. and D.W. designed the experiments. D.W., B.T. and Y.S. performed the experiments. Q.H. and D.W. analyzed the data. Q.H. wrote the manuscript.

## Declaration of competing interest

The authors declare no competing interests.

## Data availability

Data will be made available on request.

## Acknowledgements

We thank Drs. Yi Yang (East China University of Science and Technology, China) and Wang Wang (University of Washington, US) for providing indicators. We thank Junsheng Zhu for technical support.

## Appendix A. Supplementary data

Supplementary data to this article can be found online at https://doi.org/10.1016/j.redox.2022.102519.

## References

[1] G.A. Roth, G.A. Mensah, C.O. Johnson, G. Addolorato, E. Ammirati, L.M. Baddour, N.C. Barengo, A.Z. Beaton, E.J. Benjamin, C.P. Benziger, A. Bonny, M. Brauer, M. Brodmann, T.J. Cahill, J. Carapetis, A.L. Catapano, S.S. Chugh, L.T. Cooper, J. Coresh, M. Criqui, N. DeCleene, K.A. Eagle, S. Emmons-Bell, V.L. Feigin, J. Fernandez-Sola, G. Fowkes, E. Gakidou, S.M. Grundy, F.J. He, G. Howard, F. Hu, L. Inker, G. Karthikeyan, N. Kassebaum, W. Koroshetz, C. Lavie, D. Lloyd-Jones, H. S. Lu, A. Mirijello, A.M. Temesgen, A. Mokdad, A.E. Moran, P. Muntner, J. Narula, B. Neal, M. Ntsekhe, G. Moraes de Oliveira, C. Otto, M. Owolabi, M. Pratt, S. Rajagopalan, M. Reitsma, A.L.P. Ribeiro, N. Rigotti, A. Rodgers, C. Sable, S. Shakil, K. Sliwa-Hahnle, B. Stark, J. Sundstrom, P. Timpel, I.M. Tleyjeh, M. Valgimigli, T. Vos, P.K. Whelton, M. Yacoub, L. Zuhlke, C. Murray, V. Fuster, Group G-N-JGBoCDW, Global burden of cardiovascular diseases and risk factors, 1990-2019: update from the GBD 2019 study, J. Am. Coll. Cardiol. 76 (2020) 2982–3021.

[2] N.L. Bragazzi, W. Zhong, J. Shu, A. Abu Much, D. Lotan, A. Grupper, A. Younis, H. Dai, Burden of heart failure and underlying causes in 195 countries and territories from 1990 to 2017, Eur J Prev Cardiol 28 (2021) 1682–1690.

[3] R. Tian, W.S. Colucci, Z. Arany, M.M. Bachschmid, S.W. Ballinger, S. Boudina, J. E. Bruce, D.W. Busija, S. Dikalov, G.W. Dorn, , II, Z.S. Galis, R.A. Gottlieb, D. P. Kelly, R.N. Kitsis, M.J. Kohr, D. Levy, E.D. Lewandowski, J.M. McClung, D. Mochly-Rosen, K.D. O'Brien, B. O'Rourke, J.Y. Park, P. Ping, M.N. Sack, S. S. Sheu, Y. Shi, S. Shiva, D.C. Wallace, R.G. Weiss, H.J. Vernon, R. Wong, L. Schwartz Longacre, Unlocking the secrets of mitochondria in the cardiovascular system: path to a cure in heart failure-A report from the 2018 national heart, lung, and blood Institute workshop, Circulation 140 (2019) 1205–1216.

[4] K.D. O'Brien, R. Tian, Boosting mitochondrial metabolism with dietary supplements in heart failure, Nat. Rev. Cardiol. 18 (2021) 685–686.

[5] G.D. Lopaschuk, Q.G. Karwi, R. Tian, A.R. Wende, E.D. Abel, Cardiac energy metabolism in heart failure, Circ. Res. 128 (2021) 1487–1513.

[6] B. Zhou, R. Tian, Mitochondrial dysfunction in pathophysiology of heart failure, J. Clin. Invest. 128 (2018) 3716–3726.

[7] M. Tong, D. Zablocki, J. Sadoshima, The role of Drp1 in mitophagy and cell death in the heart, J. Mol. Cell. Cardiol. 142 (2020) 138–145.

[8] M. Song, A. Franco, J.A. Fleischer, L. Zhang, G.W. Dorn, 2nd. Abrogating mitochondrial dynamics in mouse hearts accelerates mitochondrial senescence, Cell Metabol. 26 (2017), 872-883 e5.

[9] Y. Ikeda, A. Shirakabe, Y. Maejima, P. Zhai, S. Sciarretta, J. Toli, M. Nomura, K. Mihara, K. Egashira, M. Ohishi, M. Abdellatif, J. Sadoshima, Endogenous Drp1 mediates mitochondrial autophagy and protects the heart against energy stress, Circ. Res. 116 (2015) 264–278.

[10] A. Shirakabe, P. Zhai, Y. Ikeda, T. Saito, Y. Maejima, C.P. Hsu, M. Nomura, K. Egashira, B. Levine, J. Sadoshima, Drp1-Dependent mitochondrial autophagy plays a protective role against pressure overload-induced mitochondrial dysfunction and heart failure, Circulation 133 (2016) 1249–1263.

[11] K. Tsushima, H. Bugger, A.R. Wende, J. Soto, G.A. Jenson, A.R. Tor, R. McGlauflin, H.C. Kenny, Y. Zhang, R. Souvenir, X.X. Hu, C.L. Sloan, R.O. Pereira, V.A. Lira, K. W. Spitzer, T.L. Sharp, K.I. Shoghi, G.C. Sparagna, E.A. Rog-Zielinska, P. Kohl, O. Khalimonchuk, J.E. Schaffer, E.D. Abel, Mitochondrial reactive oxygen species in lipotoxic hearts induce post-translational modifications of AKAP121, DRP1, and OPA1 that promote mitochondrial fission, Circ. Res. 122 (2018) 58–73.

[12] Q. Hu, H. Zhang, N. Gutierrez Cortes, D. Wu, P. Wang, J. Zhang, J.A. Mattison, E. Smith, L.F. Bettcher, M. Wang, E.G. Lakatta, S.S. Sheu, W. Wang, Increased Drp1 acetylation by lipid overload induces cardiomyocyte death and heart dysfunction, Circ. Res. 126 (2020) 456–470.

[13] W. Wang, C. Fernandez-Sanz, S.S. Sheu, Regulation of mitochondrial bioenergetics by the non-canonical roles of mitochondrial dynamics proteins in the heart, Biochim. Biophys. Acta, Mol. Basis Dis. 1864 (2018) 1991–2001.

[14] S. Xu, P. Wang, H. Zhang, G. Gong, N. Gutierrez Cortes, W. Zhu, Y. Yoon, R. Tian, W. Wang, CaMKII induces permeability transition through Drp1 phosphorylation during chronic beta-AR stimulation, Nat. Commun. 7 (2016), 13189.

[15] B.D. Paul, S.H. Snyder, Protein sulfhydration, Methods Enzymol. 555 (2015) 79–90.

[16] Z. Li, D.J. Polhemus, D.J. Lefer, Evolution of hydrogen sulfide therapeutics to treat cardiovascular disease, Circ. Res. 123 (2018) 590–600.

[17] K. Kondo, S. Bhushan, A.L. King, S.D. Prabhu, T. Hamid, S. Koenig, T. Murohara, B. L. Predmore, G. Gojon, Sr ., G. Gojon Jr., R. Wang, N. Karusula, C.K. Nicholson, J. W. Calvert, D.J.H. Lefer, (2)S protects against pressure overload-induced heart failure via upregulation of endothelial nitric oxide synthase, Circulation 127 (2013) 1116–1127.

[18] J. Kang, Z. Li, C.L. Organ, C.M. Park, C.T. Yang, A. Pacheco, D. Wang, D.J. Lefer, M. Xian, pH-controlled hydrogen sulfide release for myocardial ischemia-reperfusion injury, J. Am. Chem. Soc. 138 (2016) 6336–6339.

[19] D. Wu, Q. Hu, Y. Xiong, D. Zhu, Y. Mao, Y.Z. Zhu, Novel H2S-NO hybrid molecule (ZYZ-803) promoted synergistic effects against heart failure, Redox Biol. 15 (2018) 243–252.

[20] D. Wu, Q. Hu, X. Liu, L. Pan, Q. Xiong, Y.Z. Zhu, Hydrogen sulfide protects against apoptosis under oxidative stress through SIRT1 pathway in H9c2 cardiomyocytes, Nitric Oxide 46 (2015) 204–212.

[21] D. Wu, Q. Hu, B. Tan, P. Rose, D. Zhu, Y.Z. Zhu, Amelioration of mitochondrial dysfunction in heart failure through S-sulfhydration of Ca(2+)/calmodulin-dependent protein kinase II, Redox Biol. 19 (2018) 250–262.

[22] A.K. Mustafa, M.M. Gadalla, S.H. Snyder, Signaling by gasotransmitters, Sci. Signal. 2 (2009) re2.

[23] B. Tan, S. Jin, J. Sun, Z. Gu, X. Sun, Y. Zhu, K. Huo, Z. Cao, P. Yang, X. Xin, X. Liu, L. Pan, F. Qiu, J. Jiang, Y. Jia, F. Ye, Y. Xie, Y.Z. Zhu, New method for quantification of gasotransmitter hydrogen sulfide in biological matrices by LC-MS/MS, Sci. Rep. 7 (2017), 46278.

[24] Q. Hu, D. Wu, M. Walker, P. Wang, R. Tian, W. Wang, Genetically encoded biosensors for evaluating NAD(+)/NADH ratio in cytosolic and mitochondrial compartments, Cell Rep Methods (2021) 1.

[25] Z. Altaany, Y. Ju, G. Yang, R. Wang, The coordination of S-sulfhydration, S-nitrosylation, and phosphorylation of endothelial nitric oxide synthase by hydrogen sulfide, Sci. Signal. 7 (2014) ra87.

[26] C.F. Lee, J.D. Chavez, L. Garcia-Menendez, Y. Choi, N.D. Roe, Y.A. Chiao, J. S. Edgar, Y.A. Goo, D.R. Goodlett, J.E. Bruce, R. Tian, Normalization of NAD+ redox balance as a therapy for heart failure, Circulation 134 (2016) 883–894.

[27] D.B. Zorov, C.R. Filburn, L.O. Klotz, J.L. Zweier, S.J. Sollott, Reactive oxygen species (ROS)-induced ROS release: a new phenomenon accompanying induction of the mitochondrial permeability transition in cardiac myocytes, J. Exp. Med. 192 (2000) 1001–1014.

[28] G. Yang, L. Wu, B. Jiang, W. Yang, J. Qi, K. Cao, Q. Meng, A.K. Mustafa, W. Mu, S. Zhang, S.H. Snyder, R. Wang, H2S as a physiologic vasorelaxant: hypertension in mice with deletion of cystathionine gamma-lyase, Science 322 (2008) 587–590.

[29] D. Shao, S.C. Kolwicz Jr., P. Wang, N.D. Roe, O. Villet, K. Nishi, Y.A. Hsu, G. V. Flint, A. Caudal, W. Wang, M. Regnier, R. Tian, Increasing fatty acid oxidation prevents high-fat diet-induced cardiomyopathy through regulating parkin-mediated mitophagy, Circulation 142 (2020) 983–997.

[30] M. Valera-Alberni, M. Joffraud, J. Miro-Blanch, J. Capellades, A. Junza, L. Dayon, A. Nunez Galindo, J.L. Sanchez-Garcia, A. Valsesia, A. Cercillieux, F. Sollner, A. G. Ladurner, O. Yanes, C. Canto, Crosstalk between Drp1 phosphorylation sites during mitochondrial remodeling and their impact on metabolic adaptation, Cell Rep. 36 (2021), 109565.

[31] S.I. Bibli, J. Hu, M. Looso, A. Weigert, C. Ratiu, J. Wittig, M.K. Drekolia, L. Tombor, V. Randriamboavonjy, M.S. Leisegang, P. Goymann, F. Delgado Lagos, B. Fisslthaler, S. Zukunft, A. Kyselova, A.F.O. Justo, J. Heidler, D. Tsilimigras, R. P. Brandes, S. Dimmeler, A. Papapetropoulos, S. Knapp, S. Offermanns, I. Wittig, S. L. Nishimura, F. Sigala, I. Fleming, Mapping the endothelial cell S-sulfhydrome highlights the crucial role of integrin sulfhydration in vascular function, Circulation 143 (2021) 935–948.

[32] B.D. Paul, S.H. Snyder, H2S: a novel gasotransmitter that signals by sulfhydration, Trends Biochem. Sci. 40 (2015) 687–700.
[33] D.H. Cho, T. Nakamura, J. Fang, P. Cieplak, A. Godzik, Z. Gu, S.A. Lipton, S-nitrosylation of Drp1 mediates beta-amyloid-related mitochondrial fission and neuronal injury, Science 324 (2009) 102–105.
[34] V. Shoshan-Barmatz, A. Shteinfer-Kuzmine, A. Verma, VDAC1 at the intersection of cell metabolism, apoptosis, and diseases, Biomolecules 10 (2020).
[35] V. Shoshan-Barmatz, E.N. Maldonado, Y. Krelin, VDAC1 at the crossroads of cell metabolism, apoptosis and cell stress, Cell Stress 1 (2017) 11–36.
[36] D. Ben-Hail, R. Begas-Shvartz, M. Shalev, A. Shteinfer-Kuzmine, A. Gruzman, S. Reina, V. De Pinto, V. Shoshan-Barmatz, Novel compounds targeting the mitochondrial protein VDAC1 inhibit apoptosis and protect against mitochondrial dysfunction, J. Biol. Chem. 291 (2016) 24986–25003.
[37] Y.H. Liu, M. Lu, Z.Z. Xie, F. Hua, L. Xie, J.H. Gao, Y.H. Koh, J.S. Bian, Hydrogen sulfide prevents heart failure development via inhibition of renin release from mast cells in isoproterenol-treated rats, Antioxidants Redox Signal. 20 (2014) 759–769.
[38] A. Corvino, B. Severino, F. Fiorino, F. Frecentese, E. Magli, E. Perissutti, V. Santagada, M. Bucci, G. Cirino, G. Kelly, L. Servillo, G. Popowicz, A. Pastore, G. Caliendo, Fragment-based de novo design of a cystathionine gamma-lyase selective inhibitor blocking hydrogen sulfide production, Sci. Rep. 6 (2016), 34398.
[39] B.D. Paul, S.H. Snyder, K. Kashfi, Effects of hydrogen sulfide on mitochondrial function and cellular bioenergetics, Redox Biol. 38 (2021), 101772.
[40] A. Nishimura, K. Shimoda, T. Tanaka, T. Toyama, K. Nishiyama, Y. Shinkai, T. Numaga-Tomita, D. Yamazaki, Y. Kanda, T. Akaike, Y. Kumagai, M. Nishida, Depolysulfidation of Drp1 induced by low-dose methylmercury exposure increases cardiac vulnerability to hemodynamic overload, Sci. Signal. 12 (2019).
[41] T. Ida, T. Sawa, H. Ihara, Y. Tsuchiya, Y. Watanabe, Y. Kumagai, M. Suematsu, H. Motohashi, S. Fujii, T. Matsunaga, M. Yamamoto, K. Ono, N.O. Devarie-Baez, M. Xian, J.M. Fukuto, T. Akaike, Reactive cysteine persulfides and S-polythiolation regulate oxidative stress and redox signaling, Proc. Natl. Acad. Sci. U. S. A. 111 (2014) 7606–7611.
[42] T. Akaike, T. Ida, F.Y. Wei, M. Nishida, Y. Kumagai, M.M. Alam, H. Ihara, T. Sawa, T. Matsunaga, S. Kasamatsu, A. Nishimura, M. Morita, K. Tomizawa, A. Nishimura, S. Watanabe, K. Inaba, H. Shima, N. Tanuma, M. Jung, S. Fujii, Y. Watanabe, M. Ohmuraya, P. Nagy, M. Feelisch, J.M. Fukuto, H. Motohashi, Cysteinyl-tRNA synthetase governs cysteine polysulfidation and mitochondrial bioenergetics, Nat. Commun. 8 (2017) 1177.